Supplemental Methods:

Protein purification and labeling

Myosin: Bovine cardiac myosin was purified following procedures based on Margossian et al. [1]. Cow hearts were obtained on wet ice from *Pel-Freez*. The entire purification process was performed in a 4 ºC cold room. A thorough description is given in our previous publications [2].

HMM digestion: Myosin prepared as described in Rohde et al. [2] was thawed and brought to 2 mM $MgCl_2$ in its freezing buffer before digestion to HMM with α-chymotrypsin (*Sigma-Aldrich*, 0.025 mg/ml final concentration) for 10 minutes at 25 ºC, followed by addition of pefabloc (*Roche*, 5 mM final concentration) and then dialyzed into 10 mM Tris pH 7.5 with 2 mM $MgCl_2$ and then purified by Q-sephadex ion-exchange chromatography. The column was equilibrated in 10 mM Tris pH 8.0 at 4.0 C, the digested myosin loaded and then eluted in a gradient of 0-300 mM KCl, 10 mM Tris pH 8.0, over 300 mL at 1.5 mL/min, collecting 4 mL fractions (AKTA Prime Plus, GE). Fractions were evaluated by SDS-Page and those containing intact HMM without contaminants, pooled for experiments. The pooled HMM was dialyzed into buffers utilized for each experiment.

RLC: Expression, labeling and storage of recombinant Bovine ventricular regulatory light chain with a single engineered cysteine at position 105, is described in our previous work [2].

Actin: Actin was purified from rabbit skeletal muscle by acetone dehydration followed by extraction into ice cold water as described in our previous work [3] and then polymerized in 10 mM Tris pH 7.5, 2 mM $MgCl_2$, 0.5 mM ATP and stored on ice prior to use. Prior to use, the F-actin was stabilized with a 1:1.3 stochiometric excess of phalloidin (*Sigma Aldrich*), followed by 48 h dialysis (3 buffer changes) into 10 mM Tris pH 7.0 with 2 mM $MgCl_2$.

Protein and dye concentration: The Bradford protein concentration assay utilizing a known BSA protein standard was used throughout this study to determine protein concentrations. Reagents for this assay were purchased from *Biorad*. The extinction coefficient for the AF488 dye is 73,000 at 495 nm, and for Cy3 is 136,000 at 570 nm, per the manufacturer's specifications.

Exchange: We exchanged the AF488-labeled RLC onto HMM by combining the two proteins (4.5 molar excess RLC to HMM) in 50 mM Tris pH 7.5, 120 mM KCl, 2 mM DTT, 12 mM EDTA [4] and then incubated the reaction mix for 30 minutes at 30ºC. After the incubation, we adjusted the reaction to 12 mM $MgCl_2$ and then incubated the mixture on ice for 15 minutes followed by dialysis into 10 mM Tris pH 7.0, 30 mM KCl, 2 mM $MgCl_2$ prior to gel filtration to remove free RLC.

Buffers and solutions: All experiments, unless otherwise noted, were performed in 10 mM Tris pH 7.5, 2 mM $MgCl_2$ at 25 ºC.

Chemicals: Mavacamten (Myk-461) was custom synthesized by EAG Laboratories; purity was >97% by proton nuclear magnetic resonance (^{1}H NMR) and 99.36% by liquid chromatography/mass spectrometry (LC/MS). ATP (Adenosine 5'-triphosphate disodium salt hydrate, Grade 1 >99 %) and ADP (Adenosine 5'-diphosphate sodium >95 %) were purchased from *Sigma Aldrich*. Mant-ATP (2'-(or-3')-O-(N-methylanthraniloyl) adenosine 5'-triphosphate, trisodium salt) was purchased from *Thermo Fisher Scientific*. All other chemicals where purchased from *Sigma Aldrich*.

Steady-state ATPase activity: We measured the actin-activated MgATPase activity of the purified cardiac myosin HMM using an NADH-coupled assay [5] performed at 25 ºC in 10 mM Tris pH 7.5, 2 mM $MgCl_2$. The reaction mix contained varied [actin], and 0.2 mM NADH, 0.5 mM PEP, 2.1 mM ATP, 10 U/mL LDH, 40 U/mL PK, HMM (200 nM). We acquired absorbance at 340 nm every 10 seconds for 120 seconds total using a Beckman-Coulter DU640B spectrophotometer.

Transient kinetics: Transient biochemical experiments with steady-state fluorescence (total fluorescence intensity) detection were performed on an *Applied Photophysics* stopped-flow spectrophotometer capable of sequential mixing experiments with water bath temperature control. All experiments performed at 25 °C unless otherwise stated. The single-mix dead time for this instrument is 1.3 ms, calibrated using fluorescence enhancement

of 8-hydroxyquinoline following Mg^{+2} binding under pseudo first-order kinetics conditions [6]. All buffers were filtered and then degassed for 30 minutes under high-vacuum prior to use.

Transient time-resolved FRET (millisecond-resolved transient biochemical experiments with nanosecond-resolved fluorescence detection), $(TR)^2$FRET, was measured using a transient time-resolved fluorescence spectrophotometer [7-9]. This instrument utilizes a *Biologic USA* SFM/20 single-mix stopped-flow accessory coupled to our transient time-resolved fluorescence spectrophotometer. The dead time for the instrument was 1.8 ms, calibrated using the 8-hydroxyquinoline + Mg^{+2} control reaction [6]. For experiments mixing equilibrated myosin in the presence of 10 molar excess ATP with actin containing 1 mM MgATP, we loaded the actin into syringe A, followed by a freshly prepared 600 μL mixture of myosin + Cy3-ATP in syringe B and then immediately mixed with the actin in syringe A.

Single-turnover experiments with mant-ATP were performed with a sequential stopped flow. For mant-ATP: excitation at 280 nm and detection through a 400 nm long-pass filter.

Pyreneiodoacetimide (PIA) labeled actin was prepared as described in [10]. Pyrene-actomyosin association in the absence of nucleotide, pyrene-actomyosin dissociation in the presence of 50-molar excess of unlabeled actin, and ATP-induced dissociation of actomyosin was performed as described in [5].

Hydrolysis of ATP: We detected free phosphate in solution as described in [11]. 12.5 μM cardiac HMM (25 μM heads) was manually mixed with 20 μM ATP (Sigma-Aldrich), allowed to incubate for 5.0 seconds and quenched with 0.6 M perchloric acid, and detected with malachite green as described in [12]. Experiments were performed at room temperature, 22-23 °C.

Time-resolved fluorescence resonance energy transfer (TR-FRET) and transient TR-FRET, $(TR)^2$FRET: Fit parameters of the two-distance model are given in **Table S1** and a detailed description of data fitting is described in Rohde et al. [2].

$(TR)^2$FRET: The TRF and $(TR)^2$F spectrometers, originally described in our previous work [7-9], transiently digitize the time-resolved fluorescence emission following a 1 ns laser pulse. The laser used in this study is an artisanal 473 nm microchip laser (FP2-473-3-5) with an LD-702 controller hand crafted by *Concepts Research Corporation*, in WI, operating at 5 KHz repetition frequency. Thus samples are excited every 0.2 ms. For equilibrium and steady-state biochemical conditions, 1000 replicate waveforms were signal-averaged prior to analysis. For transient time-resolved measurements acquired after rapid mixing by stopped-flow, 5 waveforms were averaged every 1 ms. Total time-resolved fluorescence was measured with the emission polarizer set to the magic angle (54.7°) or removed.

$(TR)^2$FRET Data Analysis

Total fluorescence: We determined the total fluorescence emission for FRET samples by integrating the $(TR)^2$FRET waveforms over the nanosecond decay time after subtracting the pre-trigger dark current, ~5% in amplitude compared to the maximum waveform intensity.

TR-FRET: TRF waveforms from donor and FRET-labeled samples were analyzed as described in our previous publications [7-9] Eq. 1-13, paraphrased below. The measured time-resolved fluorescence waveform, $I(t)$ (Eq 1),

$$I(t) = \int_{-\infty}^{\infty} \mathrm{IRF}(t - t') \cdot F(t')dt' \qquad \text{Eq. 1}$$

is a function of the nanosecond decay time, t, and is modeled as the convolution integral of the measured instrument response function, IRF(t), and the fluorescence decay model, $F(t)$. The fluorescence decay model (Eq. 2)

$$F(t) = x_{\mathrm{D}} F_{\mathrm{D}}(t) + (1 - x_{\mathrm{D}})\, F_{\mathrm{DA}}(t) \qquad \text{Eq. 2}$$

is a linear combination of a donor-only fluorescence decay function, $F_{\mathrm{D}}(t)$ and an energy transfer-affected donor fluorescence decay, $F_{\mathrm{DA}}(t)$. The donor decay $F_{\mathrm{D}}(t)$ is a sum of exponentials (Eq. 3)

$$F_{\mathrm{D}}(t) = \sum_{i=1}^{2} A_{\mathrm{i}}\, exp(-t/\tau_{\mathrm{i}}) \qquad \text{Eq. 3}$$

with discrete lifetime species τ_i and pre-exponential mole fractions A_i. For the Alexa-488 donor two exponentials were required to fit the observed fluorescence. The energy transfer-affected donor decay function, $F_{DA}(t)$ (Eq. 4),

$$F_{DA}(t) = \sum_{j=1}^{2} X_j \cdot T_j(t) \quad \text{Eq. 4}$$

is a sum over multiple structural states (j) with mole fractions X_j, represented by FRET-affected donor fluorescence decays $T_j(t)$. The increase in the donor decay rate (inverse donor lifetime) due to FRET is given by the Förster equation

$$k_{Ti} = k_{Di}(R/R_{0i})^{-6}, \text{ where} \quad \text{Eq. 5}$$

$$k_{DAi} = k_{Di} + k_{Ti}, \text{and} \quad \text{Eq. 6}$$

$$k_{Di} = 1/\tau_i \quad \text{Eq. 7}$$

We modeled TR-FRET assuming that each structural state j (Eq. 4) corresponds to a Gaussian distribution of interprobe distances, $\rho_j(R)$:

$$T_j(t) = \int_{-\infty}^{\infty} \rho_j(R) \cdot \sum_{i=1}^{3} A_i \, exp\left(\frac{-t}{\tau_i} \cdot \left[1 + \left(\frac{R_{0i}}{R}\right)^6\right]\right) dR \quad \text{Eq. 8}$$

$$\rho_j(R) = \frac{1}{\sigma_j\sqrt{2\pi}} \exp\left(\frac{-\left[R - R_j\right]^2}{2\sigma_j^2}\right) \quad \text{Eq. 9}$$

$$\sigma_j = \text{FWHM}_j/\left(2\sqrt{2\ln 2}\right) \quad \text{Eq. 10}$$

As with our previous work [7-9] , R_{0i} is calculated according to Eq. 11 from the spectral overlap integral, J, the orientation-sensitive term κ^2, the refractive index n, and the donor quantum yield Q_{Di} (Eq. 12-14). $\langle Q_D \rangle$ was measured as 0.91 ± 0.01, by comparison to a quinine sulfate fluorescence standard in 50 mM H_2SO_4 at 25°C according to Eq. 14 (1, 4).

$$R_{0i} = 9780[J(\lambda)\kappa^2 n^{-4} Q_i]1/6 \quad \text{Eq. 11}$$

$$Q_{Di} = \langle Q_D \rangle \cdot \tau_i/\langle \tau \rangle \quad \text{Eq. 12}$$

$$\langle \tau \rangle = \frac{\sum_{i=1}^{3} A_i \tau_i}{\sum_{i=1}^{3} A_i} \quad \text{Eq. 13}$$

$$\langle Q_D \rangle = Q_S \cdot \left(\frac{F_D(\lambda)}{A_D(\lambda)}\right) \Big/ \left(\frac{F_S(\lambda)}{A_S(\lambda)}\right) \quad \text{Eq. 14}$$

Together, the donor fluorescence (A_i, τ_i) and distance terms (R_j, σ_j) in our analysis were shared globally between all waveforms containing FRET-labeled samples. R_j and σ_j were allowed to vary between 0.5 nm and 15.0 nm. The average Alexa-488/CY3 R_0, (6.7 nm in this study) was determined according to Eq. 11-14. The distance-dependent terms R_j (Eq.9) and σ_j (Eq. 10) define unique structural states of the LCD. The mole fraction terms X_j were allowed to vary independently in each waveform. Thus, changes in X_j reflect changes in the relative populations of the structural states (j) as the biochemical state is varied under equilibrium, steady-state, or transient conditions.

We determined the number of donor lifetimes (i) and structural states (j) that are present in each sample by fitting a set of models with the number of donor lifetime states, i increasing from 1 to 4, and the number of structural states, j, increasing from 1 to 4. For each model we test a distribution of energy transfer rates, with σ_j allowed to

vary, as well as discrete energy transfer rates where $\sigma \rightarrow 0$. The final model ($i_{max} = 2, j_{max} = 2, \sigma > 0$) was determined by evaluating the dependence of the minimized χ^2 on the number of free parameters in the global model and by the resolution of the χ^2 error surface support plane with a confidence intervals of 67%.

Table S1. Steady-state and transient kinetics measured in this paper. HMM and DMSO, S1 and DMSO, HMM and 10 μM Mava, S1 and 10 μM Mava.
Student's T-Test reporting: N.S. for $p > 0.05$, * for $p \leq 0.05$, ** for $p \leq 0.01$, *** for $p \leq 0.001$. N.C. for not compared.

Experiment, Parameters	**Myosin fragment, ± DMSO or Mava**		**Stat. signif.**
HMM steady-state, actin-activated NADH-coupled ATPase	**HMM, DMSO**	**HMM, Mava**	
k_{cat} (s^{-1}), *n=6, Error of 3 fit hyperbolas.*	2.02 ± 0.12	0.48 ± 0.04	***
$K_{0.5,Actin}$ (μM)	17.6 ± 2.8	35.3 ± 6.3	*
Mavacamten EC_{50} (μM), *n=4*	N/A	0.23 ± 0.02	N.C.
S1 steady-state, actin-activated NADH-coupled ATPase	**S1, DMSO**	**S1, Mava**	
k_{cat} (s^{-1}), *n=6, Error of 3 fit hyperbolas.*	3.64 ± 0.41	1.35 ± 0.08	***
$K_{0.5,Actin}$ (μM)	24.4 ± 7.4	20.6 ± 3.1	N.S.
Mavacamten EC_{50} (μM)	N/A	0.41 ± 0.02	N.C.
HMM steady-state, basal NADH-coupled ATPase	**HMM, DMSO**	**HMM, Mava**	
Activity (s^{-1}), *Repli.: n=3, Error:* ± *SEM.*	0.016 ± 0.005	0.003 ± 0.001	*
S1 steady-state, basal NADH-coupled ATPase	**S1, DMSO**	**S1, Mava**	
Activity (s^{-1}) , *Repli.: n=3, Error:* ± *SEM.*	0.028 ± 0.007	0.006 ± 0.002	**
HMM steady-state pyrene-actin quenching	**Acto-HMM**	**Acto-S1**	
Normalized fluorescence (A.U.), *n=4, Error:* ± *SEM.*	0.29 ± 0.03	0.34 ± 0.02	N.S.
S1 steady-state pyrene-actin quenching	**ActoHMM+ATP**	**ActoS1 + ATP**	
Normalized fluorescence (A.U.), *n=4, Error:* ± *SEM.*	0.89 ± 0.02	0.95 ± 0.01	*
HMM actin-activated single-turnover of mant-ATP	**HMM, DMSO**	**HMM, Mava**	
k_{fast} (s^{-1}), *n=6, Error of 3 hyperbolic fits.*	3.80 ± 0.33	0.30 ± 0.03	***
$K_{0.5,Actin}$ (μM)	5.3 ± 1.7	2.3 ± 0.5	N.S.
k_{slow} (s^{-1})	0.55 ± 0.03	0.037 ± 0.007	***
$K_{0.5,Actin}$ (μM)	5.4 ± 1.1	4.7 ± 1.5	N.S.
A_{fast}, fraction (A.U.)	0.77 ± 0.03	0.48 ± 0.04	**
Mavacamten EC_{50} (μM)	N/A	0.36 ± 0.08	N.C.
S1 actin-activated single-turnover of mant-ATP	**S1, DMSO**	**S1, Mava**	
k_{fast} (s^{-1}), *n=6, Error of 3 hyperbolic fit.*	5.97 ± 0.80	0.80 ± 0.11	**
$K_{0.5,Actin}$ (μM)	16.1 ± 5.0	12.6 ± 4.2	N.S.
k_{slow} (s^{-1})	0.28 ± 0.04	0.089 ± 0.002	**
$K_{0.5,Actin}$ (μM)	2.7 ± 0.9	1.3 ± 0.3	N.S
A_{fast}, fraction (A.U.)	0.87 ± 0.02	0.83 ± 0.01	N.S
HMM basal single-turnover of mant-ATP	**HMM, DMSO**	**HMM, Mava**	
k_{fast} (s^{-1}), *n=9, Error:* ± *SEM.*	0.021 ± 0.003	0.0076 ± 0.0012	***
k_{slow} (s^{-1})	0.0053 ± 0.0010	0.0008 ± 0.0002	***
A_{slow}, fraction (A.U.)	0.55 ± 0.04	0.88 ± 0.01	***

S1 basal single-turnover of mant-ATP	**S1, DMSO**	**S1, Mava**	
k_{fast} (s^{-1}), *n=9, Error: ± SEM.*	0.032 ± 0.002	0.0038 ± 0.0012	***
k_{slow} (s^{-1})	0.0075 ± 0.0010	0.0013 ± 0.0003	***
A_{slow}, fraction (A.U.)	0.17 ± 0.04	0.32 ± 0.03	**
HMM basal single-turnover of ATP, chased with mant-ATP	**HMM, DMSO**	**S1, DMSO**	
k_{fast} (s^{-1}), *n=6, Error: ± SEM.*	0.028 ± 0.005	0.025 ± 0.002	N.S.
k_{slow} (s^{-1})	0.0039 ± 0.0011	0.0045 ± 0.0006	N.S.
A_{slow}, fraction (A.U.)	0.81 ± 0.02	0.27 ± 0.03	***
AF488-RLC-HMM basal single-turnover of mant-ATP	***HMM***	**AF488-HMM**	
k_{fast} (s^{-1}), *n=9 for HMM, n=4 for AF488-HMM, Error: ± SEM.*	*0.021 ± 0.003*	0.011 ± 0.002	N.S.
k_{slow} (s^{-1})	*0.0053 ± 0.0010*	0.0037 ± 0.0007	N.S.
A_{slow}, fraction (A.U.)	*0.55 ± 0.04*	0.47 ± 0.03	N.S.
HMM basal mant-ADP release	**HMM, DMSO**	**HMM, Mava**	
k_{fast} (s^{-1}), *n=9, Error: ± SEM.*	0.45 ± 0.01	0.16 ± 0.01	***
k_{slow} (s^{-1})	0.12 ± 0.01	0.025 ± 0.003	***
$Amplitude_{slow}$, fraction (A.U.)	0.37 ± 0.02	0.62 ± 0.02	***
S1 basal mant-ADP release	**S1, DMSO**	**S1, Mava**	
k_{fast} (s^{-1}), *n=9, Error: ± SEM.*	0.41 ± 0.02	0.20 ± 0.01	***
k_{slow} (s^{-1})	0.08 ± 0.01	0.04 ± 0.01	*
$Amplitude_{slow}$, fraction (A.U.)	0.30 ± 0.03	0.28 ± 0.01	N.S.
Basal mant-ATP turnover, temperature dependence **Erying equation:** $\mathbf{k = T \cdot e^{\left(\frac{-\Delta H^{\ddagger}}{RT}+b\right)}}$, $\mathbf{R = 8.314(10^{-3})kJ \cdot K^{-1} \cdot mol^{-1}}$	**HMM**	**S1**	
Fast phase: $\Delta H^{\ddagger}$ (kJ/mol), *n=4, Error of fit.*	35.3 ± 1.5	30.9 ± 3.3	N.S.
Fast phase: b, constants and $\Delta S^{\ddagger}$ (dimensionless)	5.3 ± 0.6	3.6 ± 1.4	N.S.
Slow phase: $\Delta H^{\ddagger}$ (kJ/mol)	15.9 ± 1.3	15.1 ± 8.9	N.S.
Slow phase: b, constants and $\Delta S^{\ddagger}$ (dimensionless)	-4.3 ± 0.5	-3.9 ± 3.7	N.S.
$Amplitude_{slow}$, fraction at 35 °C (A.U.) , *n=4, Error: ± SEM.*	0.51 ± 0.03	0.07 ± 0.03	***
Basal mant-ATP turnover, KCl dependence	**HMM**	**S1**	
Average k_{fast} (s^{-1}), *n=4, Error: ± SEM.*	0.022 ± 0.001	0.031 ± 0.002	**
Average k_{slow} (s^{-1})	0.0062 ± 0.0004	0.0069 ± 0.0013	N.S.
$Amplitude_{slow}$, fraction at 100 mM KCl (A.U.), *Error of fit.*	0.23 ± 0.10	0.24 ± 0.09	N.S.
Basal mant-ATP turnover, 100 mM KCl and 10 μM Mava	**HMM**	**S1**	
k_{fast} (s^{-1}), *n=4, Error: ± SEM.*	0.0037 ± 0.0008	0.0049 ± 0.0005	N.S.
k_{slow} (s^{-1})	0.0009 ± 0.0001	0.0011 ± 0.0002	N.S.
A_{slow}, fraction (A.U.)	0.59 ± 0.03	0.46 ± 0.02	*
Powerstroke, $(TR)^2$FRET, fluorescently-labeled RLC	**HMM, DMSO**	**HMM, Mava**	
Actin-induced lever arm rotation (s^{-1}), *n=6, Error of 3 fits.*	11.49 ± 0.81	4.87 ± 0.17	**
Actin-induced rotation, $K_{0.5,Actin}$ (μM)	4.20 ± 0.89	0.6 ± 0.2	*
Slow phase, lever arm rotation (s^{-1})	1.33 ± 0.24	0.43 ± 0.08	*

Slow phase, $K_{0.5,Actin}$ (μM)	3.42 ± 2.05	1.0 ± 1.3	N.S.
Maximum fit Amplitude, fast phase (normalized)	0.59 ± 0.04	0.23 ± 0.03	**
Maximum fit Amplitude, $K_{0.5,Actin}$ (μM)	5.1 ± 0.8	1.6 ± 1.0	N.S.
Distance Distribution, $(TR)^2$FRET	**HMM, DMSO**	**HMM, Mava**	
M** (Distance 1), *n=28, Error is avg. surface plane error.*	6.54 ± 0.55	Globally-fit	
FWHM 1 (nm)	1.87 ± 0.62	"	
M* (Distance 2) (nm)	10.53 ± 1.15	"	
FWHM 2 (nm)	2.20 ± 0.82	"	
Donor-only fluorescence, AF488, $(TR)^2$FRET	**HMM, DMSO**	**HMM, Mava**	
τ_1 (ns), *n=12, Error is avg. surface plane error.*	3.791 ± 0.008	Globally-fit	
A_1 (A.U.)	0.645 ± 0.029	"	
τ_2 (ns)	0.493 ± 0.011	"	
Pyrene-A.M diss. (50x unlabeled-actin chase)	**HMM, DMSO**	**HMM, Mava**	
k_1 (s^{-1}), *n=6, Error: ± SEM.*	0.052 ± 0.004	0.052 ± 0.006	N.S.
A_1, fraction (A.U.)	0.23 ± 0.01	0.24 ± 0.01	N.S.
k_2 (s^{-1})	0.0071 ± 0.0001	0.0075 ± 0.0001	*
Mant-ATP binding Myosin	**HMM, DMSO**	**HMM, Mava**	
k_1 (s^{-1}), *n=3, Error: ± SEM.*	24.3 ± 0.8	29.0 ± 1.0	*
A_1, fraction (A.U.)	0.69 ± 0.01	0.77 ± 0.02	*
k_2 (s^{-1})	1.42 ± 0.6	1.75 ± 0.9	N.S.
Mant-ATP binding Actomyosin	**HMM, DMSO**	**HMM, Mava**	
k_1 (s^{-1}), *n=6, Error: ± SEM.*	309 ± 110	143 ± 22	N.S.
A_1, fraction	0.27 ± 0.01	0.28 ± 0.02	N.S.
k_2 (s^{-1})	25.6 ± 0.9	20.9 ± 0.7	**
A_2, fraction	0.63 ± 0.02	0.61 ± 0.01	N.S.
k_3 (s^{-1})	6.4 ± 2.4	1.8 ± 0.3	N.S.
Mant-ADP release from actoHMM, chased with ATP	**HMM, DMSO**	**HMM, Mava**	
k_1 (s^{-1}), *n=6, Error: ± SEM.*	66.8 ± 0.8	64.5 ± 2.3	N.S.
A_1, fraction	0.93 ± 0.01	0.92 ± 0.01	N.S.
k_2 (s^{-1})	2.4 ± 0.4	2.4 ± 0.3	N.S.
Recovery stroke, $(TR)^2$FRET	**HMM, DMSO**	**HMM, Mava**	
Fast phase, ATP-induced lever arm rotation, k_{cat} (s^{-1})	58.5 ± 11.7	42.1 ± 4.7	N.S.
ATP-induced lever arm rotation $K_{0.5}$ [Cy3ATP] (μM)	10.4 ± 3.2	8.3 ± 1.5	N.S.
Slow phase, k_{cat} (s^{-1})	1.97 ± 0.38	1.24 ± 0.20	N.S.
Slow phase $K_{0.5}$ [Cy3ATP] (μM)	1.56 ± 0.93	1.29 ± 0.70	N.S.
Mavacamten EC_{50} (μM)	N/A	27.5 ± 4.7	N.C.
Steady state hydrolysis	**HMM, DMSO**	**HMM, Mava**	
[P_i] / [ATP] (no units), *n=6, Error: ± SEM.*	0.62 ± 0.03	0.55 ± 0.01	N.S.

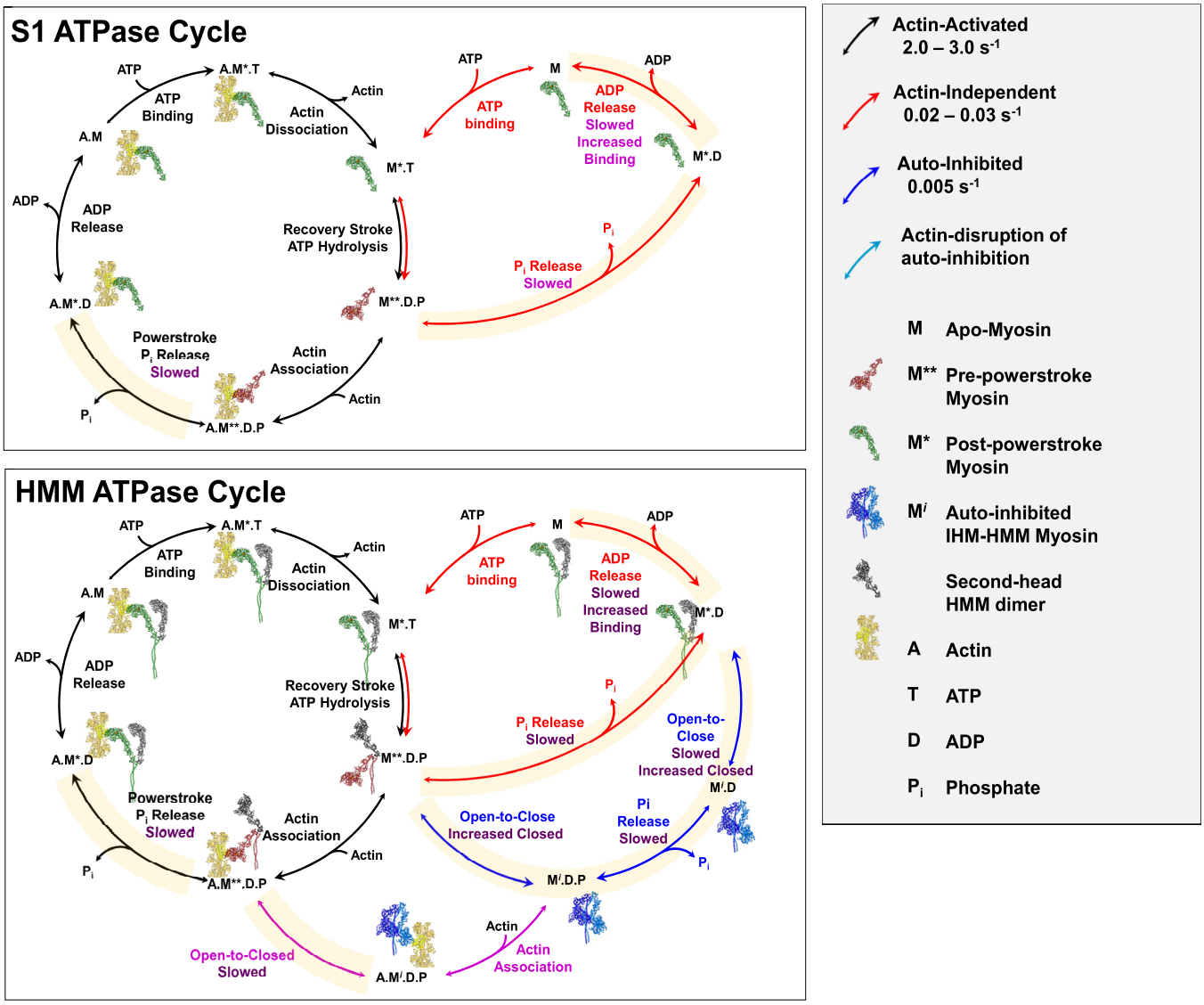

Fig. S1. Summary of predominant kinetic steps navigated by cardiac myosin in the presence of excess ATP. (Top) Steps navigated by a single S1 head during actin-independent (red arrows) or actin-activated (black arrows) ATPase cycling. (Bottom) Dominant steps navigated by an individual HMM head of the HMM dimer during actin-independent (red arrows), actin-activated (black arrows) ATPase cycling. Steps associated with auto-inhibition in the absence or actin (blue arrows). Activation of auto-inhibited HMM by actin indicated by magenta arrows. Myosin's dominant thermodynamic states indicated as defined in the figure legend. For HMM, the scheme denotes the activity of a single head. The second head is colored grey and its thermodynamic state is not considered in the model. The key steps altered by mavacamten are indicated by yellow shading. Mavacamten's relative effect on these steps are indicated in burgundy text such that "Slowed" denotes an increase in the total transit time for the step ($1/k_{forward} + 1/k_{reverse}$), "Increased Closed" denotes a shift of the equilibrium constant toward the closed auto-inhibitory state, and Increased "ADP Binding" denotes an increase in the affinity of the ATPase site for ADP. The mavacamten sensitive steps include structural transitions associated with lever-arm movement and phosphate release after ATP hydrolysis, structural changes in the nucleotide-binding pocket associated with ADP release in the absence of actin, and isomerization to an auto-inhibited structural state hypothesized to result from the interacting heads motif (open-to-closed transition).

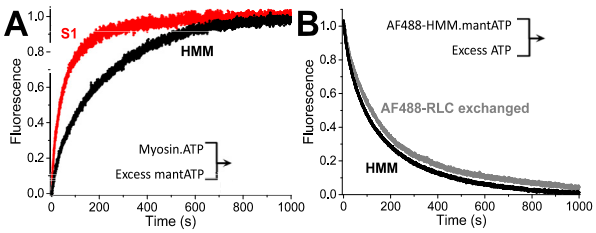

Fig. S2. Basal ATP turnover controls: Myosin.ATP mixed with mant-ATP; basal turnover with exchanged light chain. (A) To ensure the mant-nucleotide was not inducing non-physiological phenomenon in the basal mant-turnover experiments, we performed the inverse mix: incubating 0.4 μM S1 or 0.2 μM HMM with 4.0 μM ATP and then mixed with 400 μM mant-ATP. HMM remains biphasic, unlike S1. (B) Fluorescently-labeled and exchanged-on RLC, used in $(TR)^2$FRET experiments, did not disrupt the SRX-like basal ATP turnover of HMM. The same bi-phasic behavior was observed. Fits reported in Table S1.

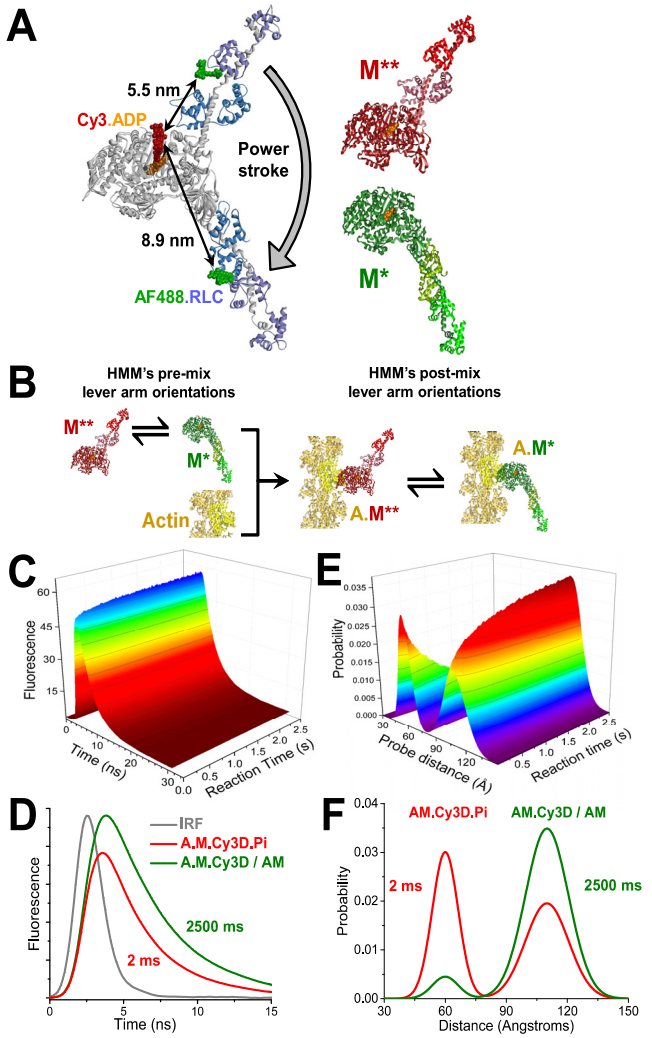

Fig. S3. Light-chain domain rotation data acquisition and analysis with $(TR)^2$FRET. (A) Fluorescently-labeled HMM, dyes modeled on perpendicular to the protein surface, PDB: 1B7T, 1DFL. Donor fluorophore is AlexaFluor488-RLC and acceptor fluorophore is Cy3-ATP. Distances represent dye center-dye center. Powerstroke occurs from the lever-up pre-powerstroke state (red myosin S1 cartoon, lever up) to the lever-down post-powerstroke state (green myosin S1 cartoon, lever down). S1 depicted for simplicity, HMM used. (B) Stopped-flow mix of myosin with actin, to detect FRET between the lever arm and catalytic domain of cardiac HMM. Equilibrium of structural states of myosin with fluorescently-labeled and exchanged-on RLC with excess fluorescent Cy3-ATP, mixed with actin, detecting the depletion of the lever-up M** structural state (red). (C) 2000 time-resolved FRET waveforms were acquired with 125 picosecond resolution. Each waveform results from after excitation with a 5000 Hz pulsed laser, acquired following stopped-flow mixing of 0.1 μM AF488-labeled cardiac HMM equilibrated with 2.0 μM Cy3-ATP, mixed with 20 mM Actin containing 1.0 mM ATP, depicting a total integrated fluorescence intensity change of 27% for the DMSO control shown. (D) The first and last time-resolved fluorescent waveforms shown in C. Laser pulse (IRF) is shown in gray. (E) Global two-distance fit to each acquired waveforms in C, depicting a mole fraction change of 0.49 for DMSO. Every waveform detected in C was fit to this two-distance model (SI Methods). (F) First and last two-distance fit shown in E.

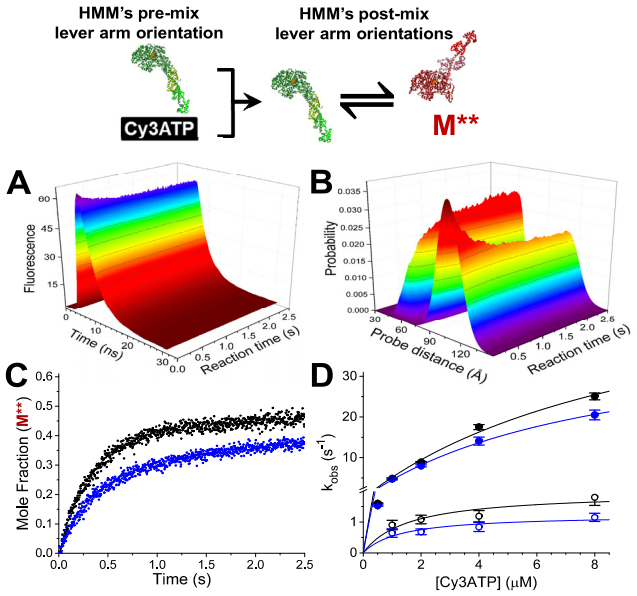

Fig. S4. Recovery stroke detected with $(TR)^2$FRET. (A) Transient time-resolved FRET waveforms acquired after mixing 0.1 μM AF488 labeled cardiac HMM with 2.0 μM Cy3-ATP, depicting a total integrated fluorescence intensity change of 25% for DMSO. Reaction mixed represented above; S1 shown for simplicity. (B) Global two-distance structural state model was fit to each acquired waveforms in A, depicting a mole fraction change of 0.46. (C) Plotted mole fraction of the M**, lever-up, post-recovery stroke structural state at 2.0 μM Cy3ATP in the absence (black) or presence (blue) of 10 μM Myk461. While our fluorescent labeling scheme is likely detecting inter-head FRET, our analysis of the power stroke and recovery stroke has focused on the rate of fluorescence change and not the structural resolution of these measurements. The distance distributions of our two-distance fits were unchanged in the presence or absence of mavacamten, and the mole fraction of myosin molecules in a pre- and post-powerstroke state were consistent in the presence and absence of mavacamten as well. These observations suggest inter-head FRET is a small contribution to the FRET changes we observe because mavacamten had no detectable effect on the fluorescence lifetimes associated with the various biochemical states in these stopped-flow experiments. (D) Observed rate constant for the recovery stroke over a range of nucleotide concentrations. $k_{obs1,DMSO}$ = $58.5s^{-1}[ATP]/(10.4\mu M+[ATP])$, $k_{obs1,Myk461}$ = $42.1s^{-1}[ATP]/(8.3\mu M+[ATP])$, $k_{obs2,DMSO}$ = $1.9s^{-1}[ATP]/(1.6\mu M+[ATP])$, $k_{obs2,Myk461}$ = $1.2s^{-1}[ATP]/(1.3\mu M+[ATP])$.

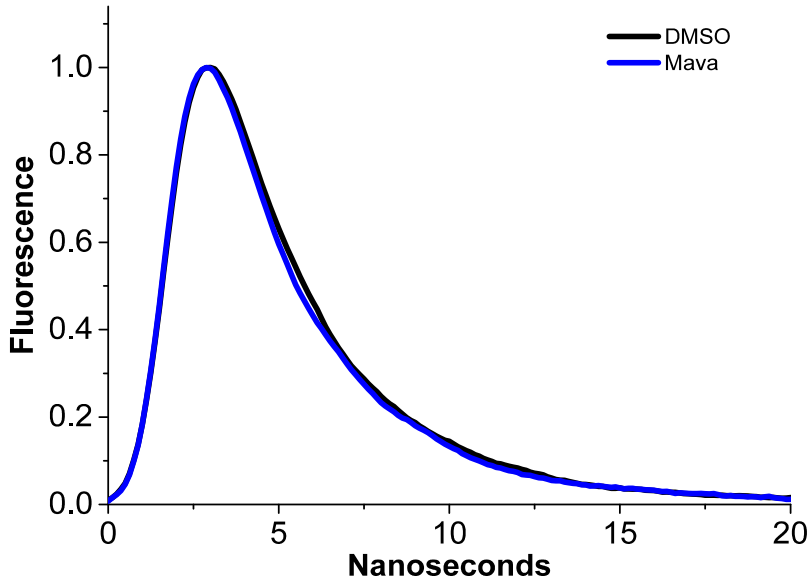

Fig. S5. Mavacamten does not change TR-FRET between AF488 labeled cardiac HMM with 2.0 μM Cy3-ATP. TR-FRET measured as described in Fig. S4 in the absence of actin and presence of 30 μM mavacamten. The difference between the average lifetimes of the depicted waveforms is 80 picoseconds +/- 10 picoseconds.

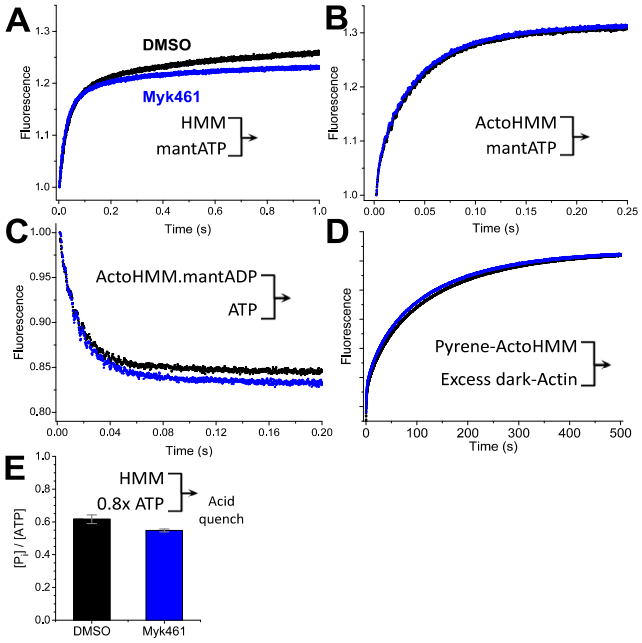

Fig. S6. Mavacamten does not change the kinetics of several steps in the myosin ATPase cycle. (A) Mant-ATP binding to HMM. 2.0 μM mant-ATP binding to 0.1 μM HMM in the presence of 1% DMSO (black) or 5.0 μM Myk461 dissolved in DMSO (blue). (B) Mant-ATP binding actoHMM. 2.0 μM mant-ATP binding pre-incubated 5.0 μM actin and 0.1 μM HMM. Observed rate constants given in Table S1. Individual, representative mixes with transients from the average of 6-10 shots of the stopped flow. Two exponential fit and error bars shown in Table S1 from n = 6 mixes, ± SEM. (C) ADP dissociation detected with 5.0 μM actin, 0.1 μM HMM and 2.0 μM mant-ADP chased with 2.0 mM non-fluorescent ATP. Black is DMSO control, blue is 5.0 μM Myk461. Observed rate constants reported in Table S1, ± SEM from n = 6 mixes. (D) Actomyosin dissociation detected with incubation of 1.5 μM pyrene-actin and 0.4 μM HMM mixed with 20 μM unlabeled-actin. Black trace is DMSO, blue is 5.0 μM Myk461. Observed rate constants reported in Table S1 ± SEM from n =6. (E) Hydrolysis detected with malachite green following acid quench with perchloric acid. 12.5 μM two-headed HMM was mixed with 20 μM ATP (5:4 stoichiometry) and incubated for 5.0 s, then quenched with 0.6 M perchloric acid and detected with malachite green. The concentration of P_i was determined with a standard curve.

References

1. Margossian, S.S. and S. Lowey, *Preparation of myosin and its subfragments from rabbit skeletal muscle.* Methods in enzymology, 1982. **85 Pt B**: p. 55-71.
2. Rohde, J.A., D.D. Thomas, and J.M. Muretta, *Heart failure drug changes the mechanoenzymology of the cardiac myosin powerstroke.* Proc Natl Acad Sci U S A, 2017. **114**(10): p. E1796-E1804.
3. Prochniewicz, E., T.F. Walseth, and D.D. Thomas, *Structural dynamics of actin during active interaction with myosin: different effects of weakly and strongly bound myosin heads.* Biochemistry, 2004. **43**(33): p. 10642-52.
4. Hopkins, S.C., et al., *Orientation changes of the myosin light chain domain during filament sliding in active and rigor muscle.* Journal of molecular biology, 2002. **318**(5): p. 1275-91.
5. De La Cruz, E.M. and E.M. Ostap, *Kinetic and equilibrium analysis of the myosin ATPase.* Methods in enzymology, 2009. **455**: p. 157-92.
6. Brissette, P., D.P. Ballou, and V. Massey, *Determination of the dead time of a stopped-flow fluorometer.* Analytical biochemistry, 1989. **181**(2): p. 234-8.
7. Muretta, J.M., K.J. Petersen, and D.D. Thomas, *Direct real-time detection of the actin-activated power stroke within the myosin catalytic domain.* Proceedings of the National Academy of Sciences of the United States of America, 2013. **110**(18): p. 7211-6.
8. Nesmelov, Y.E., et al., *Structural kinetics of myosin by transient time-resolved FRET.* Proceedings of the National Academy of Sciences of the United States of America, 2011. **108**(5): p. 1891-6.
9. Muretta, J.M., et al., *High-performance time-resolved fluorescence by direct waveform recording.* The Review of scientific instruments, 2010. **81**(10): p. 103101.
10. Kouyama, T. and K. Mihashi, *Fluorimetry study of N-(1-pyrenyl)iodoacetamide-labelled F-actin. Local structural change of actin protomer both on polymerization and on binding of heavy meromyosin.* Eur J Biochem, 1981. **114**(1): p. 33-8.
11. Sirigu, S., et al., *Highly selective inhibition of myosin motors provides the basis of potential therapeutic application.* Proc Natl Acad Sci U S A, 2016. **113**(47): p. E7448-E7455.
12. Lanzetta, P.A., et al., *An improved assay for nanomole amounts of inorganic phosphate.* Anal Biochem, 1979. **100**(1): p. 95-7.